Earth and Planetary Science Letters 432 (2015) 293–299

Contents lists available at ScienceDirect

Earth and Planetary Science Letters

www.elsevier.com/locate/epsl

P-wave velocity structure beneath Mt. Melbourne in northern Victoria Land, Antarctica: Evidence of partial melting and volcanic magma sources

Yongcheol Park, Hyun Jae Yoo *, Won Sang Lee, Choon-Ki Lee, Joohan Lee, Hadong Park, Jinseok Kim, Yeadong Kim

Korea Polar Research Institute, Incheon, South Korea

ARTICLE INFO

Article history:
Received 20 July 2015
Received in revised form 2 October 2015
Accepted 6 October 2015
Available online xxxx
Editor: P. Shearer

Keywords:
Antarctica
Mt. Melbourne
P-wave tomography
mantle edge flow
Jang Bogo Station

ABSTRACT

Mt. Melbourne is a late Cenozoic intraplate volcano located ~30 km northeast of Jang Bogo Station in Antarctica. The volcano is quiescent with fumarolic activity at the summit. To monitor volcanic activity and glacial movements near Jang Bogo Station, a seismic network was installed during the 2010–11 Antarctic summer field season. The network is maintained during the summer field season every year, and the number of stations has been increased. We used continuous seismic data recorded by the network and an Italian seismic station (TNV) at Mario Zucchelli Station to develop a 3-D P-wave velocity model for the Mt. Melbourne area based on the teleseismic P-wave tomographic method. The new 3-D model presented a relative velocity structure for the lower part of the crust and upper mantle between depths of 30 and 160 km and revealed the presence of two low-velocity anomalies beneath Mt. Melbourne and the Priestley Fault. The low-velocity anomaly beneath Mt. Melbourne may be caused by the edge flow of hot mantle material at the lithospheric step between the thick East Antarctic Craton and thin Ross Sea crust. The other low-velocity anomaly along the Priestley Fault may have been beneath Mt. Melbourne and moved to the southern tip of the Deep Freeze Range, where the crustal thickness is relatively thin. The anomaly was trapped on the fault line and laterally flowed along the fault line in the northwest direction.

1. Introduction

Mt. Melbourne is part of the McMurdo Volcanic Group in northern Victoria Land (NVL), which resulted from extensive rift-related alkaline magmatic activity between the Transantarctic Mountains and Ross Sea basin. Magmatism in NVL initiated at ~50 Ma in association with the extension of the Ross Sea basin and became more intense after ~30 Ma when the major NW–SE fault system was reactivated with Paleozoic right-lateral strike slips (Fig. 1) (Rocchi et al., 2003; Rossetti et al., 2000; Salvini et al., 1997; Storti et al., 2001). Mt. Melbourne is only ~30 km northeast of Jang Bogo Station and forms an N–S elongated stratovolcano. The total volume of the volcanic field is 250 km^3, including the surrounding volcanic field and a volume of 180 km^3 for the summit cone (Wörner and Viereck, 1989). An eruption was estimated to have occurred less than few thousand years ago based on the presence of ash layers in ice cliffs and nearby glaciers (Nathan and Schulte, 1967), and the most recent eruption occurred between 1862 and 1922 based on snow accumulation rates and the buried depth of ash layers in ice cliffs (Lyon, 1986). Current geothermal activity has been observed with warm ground in the summit area, and fumarole ice towers and pinnacles (Nathan and Schulte, 1967; Wörner and Viereck, 1989). The temperature at the summit area was 59 °C at a depth of 25 cm from the ground surface (Keys et al., 1983).

Mt. Melbourne is located on the eastern flank of the Ross Sea rift, and the location and magmatism of the volcano in NVL are generally accepted to be genetically linked to Ross Sea rifting as part of the West Antarctic Rift System (WARS) and the uplift of the Transantarctic Mountains rift shoulder. Several models have been proposed to explain the evolution history of WARS, the accompanying Cenozoic magmatism along the coastal region of the western Ross Sea margin, and the Transantarctic Mountains (inset map in Fig. 1). A mantle plume model has been suggested by several researchers to explain the low-velocity anomalies (Gupta et al., 2009; Kyle et al., 1992; Morelli and Danesi, 2004; Sieminski et al., 2003), the presence of large volumes of sub-

* Corresponding author at: Korea Polar Research Institute, 26 Songdomirae-ro, Yeonsu-gu, Incheon, 406-840, South Korea.
E-mail address: hjyoo@kopri.re.kr (H.J. Yoo).

http://dx.doi.org/10.1016/j.epsl.2015.10.015
0012-821X/

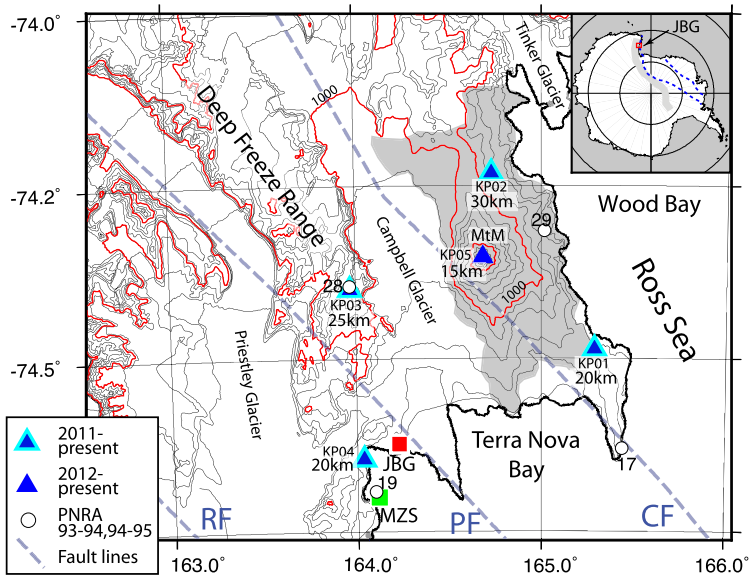

Fig. 1. Locations of the KPSN stations (red triangles) and PNRA temporary seismic stations (white circles) in the Mt. Melbourne area. The numbers at the symbols represent the Moho depths computed by receiver function studies. The digital elevation model and the free-floating boundary (thick black line) were extracted from Bamber et al. (2009) and Bindschadler et al. (2011), respectively. Inset map: the dotted blue lines indicate the boundaries of the West Antarctic Rift system, and the grey line represents the Transantarctic Mountains. JBG: Jang Bogo Station; MZS: Mario Zucchelli Station; TNV: Italian broadband seismic station in MZS; RF: Reeves Fault; PF: Priestley Fault; and CF: Campbell Fault. (For interpretation of the references to color in this figure legend, the reader is referred to the web version of this article.)

glacial and submarine volcanic rocks and its geochemical signatures (Behrendt et al., 1994, 1992; Hole and LeMasurier, 1994; Storey et al., 1999). On the other hand, more recent tomographic study has revealed that the low-velocity anomaly beneath the Ross Island and Terror Rift is constrained to the upper 200–300 km of the mantle, and there is little evidence for lower mantle upwelling beneath this region. Meanwhile, Mary Bird Land is above a deep-seated (~800 km deep) low-velocity anomaly, which has been interpreted as a mantle plume ponded below a 660 km deep discontinuity (Hansen et al., 2014). Other geological and seismological studies have suggested that the magmatism and low-velocity anomalies in the NVL are better explained by small-scale mantle convection associating with the tectonics of WARS rather than by mantle plumes (Armienti and Perinelli, 2010; Barklage et al., 2009; Faccenna et al., 2008; Rocchi et al., 2002, 2005, 2003). However, it is still unclear whether such small-scale mantle convection is dominant beneath Mt. Melbourne, which is the active volcano at the northern end of Terror Rift, because the velocity structure beneath this area has not been clearly resolved by previous seismic studies owing to insufficient resolution and the limitations of the data coverage (Hansen et al., 2014; Lawrence et al., 2006; Morelli and Danesi, 2004; Watson et al., 2006).

The first geophysical observations at Mt. Melbourne were set up in 1988 by the Italian Progetto Nazionale de Ricerche in Antartide (PNRA) program. A network of five tilt stations was installed in 1988–89 for continuous recording, and a seismic network was set up in 1990 that consisted of two short-period single-component and two short-period three-component stations constrained by a local trigger (Bonaccorso et al., 1997). Based on data from the three-component stations, 17 volcanic events were roughly located. The long-period features of the events may have been caused by the active presence of magmatic fluids in the source processes or the result of fracturing processes between brittle and plastic behaviors (Gambino and Privitera, 1996). The other seismic array was operated with three-component 5-s sensors recording continuously during the austral summers of 1993–94 and 1994–95 in the PNRA framework. Four temporary stations were located at the vertices of a square-shaped array around Mt. Melbourne, and the crustal thicknesses at each station were computed with teleseismic receiver functions (circles with crustal thickness in Fig. 1) (Di Bona et al., 1997). The latest seismic network, which is called the Korea Polar Seismic Network in Terra Nova Bay area (KPSN@TNB), was deployed by the Extreme Geophysics Group (EGG) at the Korea Polar Research Institute (KOPRI) during the 2010–11 summer field season. Currently, KPSN@TNB consists of six broadband seismic stations, and the crustal structure at each station has been studied (Fig. 1) (Yoo et al., 2015). The teleseismic events for the present study were extracted from continuous data recorded by KPSN@TNB between 2011 and 2013 and the permanent Italian broadband seismic station TNV at Mario Zucchelli station between 2011 and 2012 (Fig. 1).

This paper presents the first three-dimensional P-wave velocity structure beneath Mt. Melbourne based on using teleseismic data observed by KPSN@TNB. The model features an N–S elongated low-velocity anomaly beneath Mt. Melbourne and a linearly trending low-velocity anomaly in the NW–SE direction along the Priestley Fault. We discuss the resolution of the inverted model and the origins of the low-velocity anomalies for comparison with the results of previous studies in later sections.

2. Data and method

KPSN@TNB was installed on rock outcrops to monitor the volcanic and seismic activities in the vicinity of Mt. Melbourne, including signals from ice movements in Campbell Glacier and Priestley Glacier. The data from the KP02 and KP03 stations had electrical pulses during the winter seasons due to abnormal sensor currents when the temperature was below −20 °C. However, the waveforms from teleseismic events of ≥M5.5 were good enough to pick the first arrivals. Detailed information on the performance of KPSN@TNB is presented in a previous paper (Park et al., 2014).

We inspected over 1000 events within the epicentral distance range between 30° and 90° for P-waves and 115° and 150° for PKP phases to gain a good signal-to-noise ratio. Selected events were recorded by at least three stations. The ray coverage was biased toward the N–S axis because the majority of the events came from back-azimuth ranges between −70 and 15 and 130 to 180 (see Fig. S1). First, P- and PKP-waves were manually picked

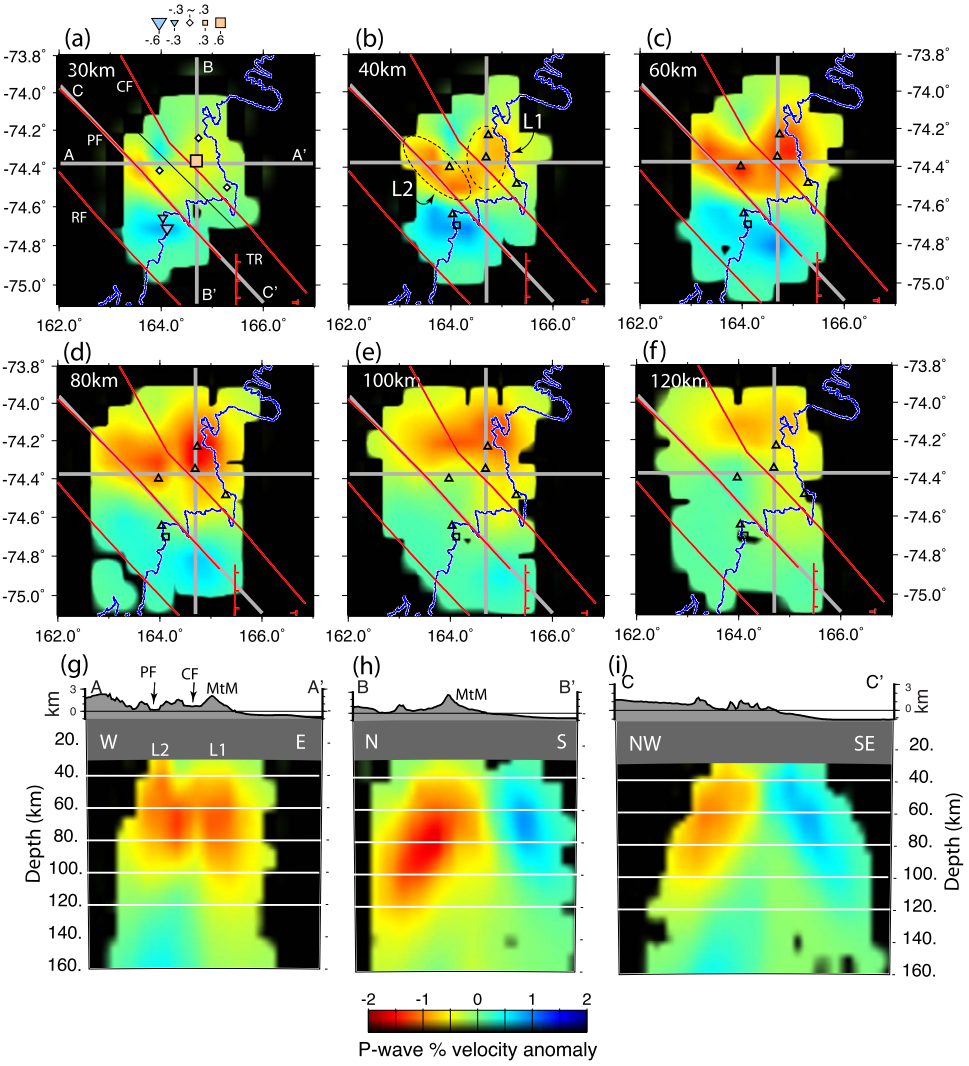

Fig. 2. P-wave tomography image. (a)–(f) Horizontal cross-sections through the model for depths of 20, 40, 60, 80, 100, and 120 km. (g)–(i) Vertical cross-sections for each line in (a). Areas with a hit count of <5 are darkened. The faults are shown as red lines. RF: Reeves Fault; PF: Priestley Fault; CF: Campbell Fault; TR: Terror Rift; MtM: Mt. Melbourne. The grey lines represent the locations of vertical cross-section profiles, and the C–C′ vertical cross-section profile is overlaid with PF.

from filtered event data with a zero-phase two-pole Butterworth filter having corner frequencies of 0.5–5 Hz. Relative travel time residuals were accurately determined with the multichannel cross-correlation (MCCC) method (VanDecar and Crosson, 1990). During the MCCC procedure, we selected a 3-s time window (1 s before and 2 s after from the manual picking time) that contained the initial arrival and typically one or two cycles of the P-wave. The mean standard deviation of the residuals was 0.025 s. After the MCCC was computed, we selected events when all cross-correlation coefficients of the pair of traces were over 0.85, and 1390 P-wave ray paths from 369 events and 111 PKP-wave ray paths from 33 events were obtained. The majority of rays from the selected events came from the NW and SE directions for P-waves (Fig. S1). Before we inverted the P-wave velocity model, we computed the relative arrival-time residuals $T_{res_{ij}} = t_{ij} - (t_{e_{ij}} - \bar{t}_{e_j})$ as a function of the back-azimuth and epicentral distance for each station (Fig. S2), where t_{ij} is the relative arrival time according to MCCC for the ith station and jth event, $t_{e_{ij}}$ is the theoretical travel time computed from the IASP91 model (Kennett and Engdahl, 1991) for the ith station and jth event, and $\bar{t}_{e_j}$ is the mean of the travel time by the IASP91 model for the jth event. The most delayed travel time residual (~1.3 s) and mean value (0.57) were observed at KP05 on the summit of Mt. Melbourne, and the residuals at KP03 also showed slow values ($\bar{T}_{res} = 0.16$ s) (see Fig. S2). The fastest relative travel time residual was observed at TNV station, and its mean residual time was −0.33 s. The different elevations of KP05 (~2576 m) and TNV (~400 m) can generate a time delay of ~0.48 s based on a shear wave velocity of 2.5 km/s and Vp/Vs ratio of 1.79 for the shallowest layer beneath KP05 station (Yoo et al., 2015), which is much less than the peak-to-peak relative residual travel time value of 0.9. Thus, we can infer that the mantle beneath Mt. Melbourne may have a slower structure than the vicinity.

We used the regularized nonlinear least-squares inversion method of VanDecar (1991) to invert a three-dimensional P-wave velocity model beneath the Mt. Melbourne area based on relative arrival-time residuals. The method represents the slowness by using a b-spline under tension that is constrained at a series of regular knots. These were parameterized to a latitude of 10 knots, longitude of 11 knots, and depth of 29 knots for the model space. The knot spaces for the latitude and longitude were 0.1° (~11.1 km) between −75.4° and −73.4° and 0.33° (~9.9 km) between 161°E and 165.1°E, respectively. The knot spaces for depth were 10 km up to a depth of 100 km and 20 km up to a depth of 340 km (see Fig. S3). We used the IASP91 model (Kennett and Engdahl, 1991) for the initial model, and the models were inverted iteratively up to 2000 times with the conjugate gradients

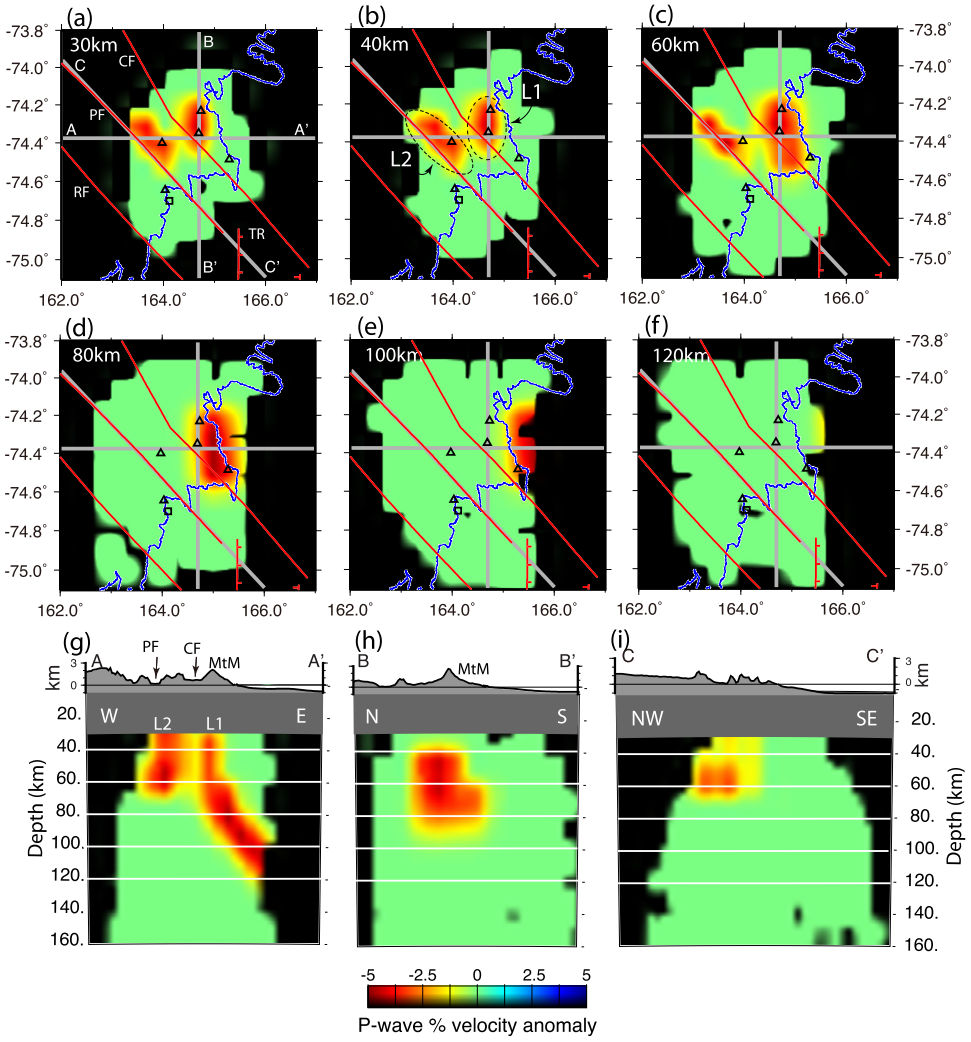

Fig. 3. Best-input model for synthetic target resolution test. Low-velocity anomalies were set by assembling 16-km-wide Gaussian spheres with a −5% peak velocity anomaly for 40–70 km depths and 20-km-wide Gaussian spheres for 70–130 km depths with 60° dipping to the east for the N–S oriented low-velocity anomaly and 23-km-wide Gaussian spheres for the NW–SE oriented anomaly. (a)–(f) Horizontal cross-sections through the model for depths of 20, 40, 60, 80, 100, and 120 km. (g)–(i) Vertical cross-sections for each line in (a).

method (VanDecar, 1991). With the regularized nonlinear least-squares inversion procedure, station static terms were computed to compensate for travel time residuals arising from the local shallow structure (see Fig. S4), and the source terms were also inverted for each event to account for first-order uncertainties in the event origin time and location and large-scale velocity heterogeneities in the source region. By investigating the tradeoff curve of the relative travel time RMS residual reduction versus the RMS model roughness, optimum smoothing and flattening parameters for the model were determined. The final model accounted for an 88% reduction in the RMS residual travel time (from 0.243 s to 0.029 s).

3. Inversion results and resolution test

Figs. 2(a)–(f) show horizontal depth slices, and Figs. 2(g)–(i) show vertical cross-sections of Fig. 2(a). The model does not show depths outside 30–160 km because of the insufficient number of crossing ray paths deeper than 160 km, and anomalies shallower than 30 km were damped out. The depth slices and vertical cross-sections through the velocity model showed a low-velocity anomaly of $\delta V_P = -1\%$ to -1.8%. The depth slices for the depth of 40–80 km (Figs. 2(b)–(d)) showed low-velocity anomalies mainly trending in the NW–SE, parallel to the Priestley Fault (L2 in Fig. 2(b)), and N–S directions beneath Mt. Melbourne (L1 in Fig. 2(b)). The low-velocity anomalies moved north with an E–W trend in the dipper depths (Figs. 2(e)–(f), (h)–(i)). The vertical slices cutting the model in the E–W direction (Fig. 2(g)) showed that the low-velocity anomaly beneath Mt. Melbourne (L1) comes from a deeper depth with an eastern dipping structure than from the depth (~90 km) of the low-velocity anomaly beneath the Priestley Fault (L2).

We performed a number of tests to examine the resolution of our model, including the checkerboard and several target structures. Our model was inverted from a limited number of rays (1309 P and 111 PKP arrivals) and could not properly resolve small structures, such as a checkerboard pattern. From the inverted model, we assumed that there were two low-velocity anomalies trending N–S (L1) and NW–SE (L2) beneath Mt. Melbourne and the Priestley Fault, respectively. However, we could not determine how they changed with increasing depth, such as the size and dipping angles, and how deep they originated. Therefore, we set two separate low-velocity anomalies like L1 and L2 (Fig. 3(b)) and performed resolution tests with synthetic travel time residuals along the ray paths computed from the model with various dipping angles and depth penetrations for the low-velocity anomalies (L1 and L2). Through several trials with different target models,

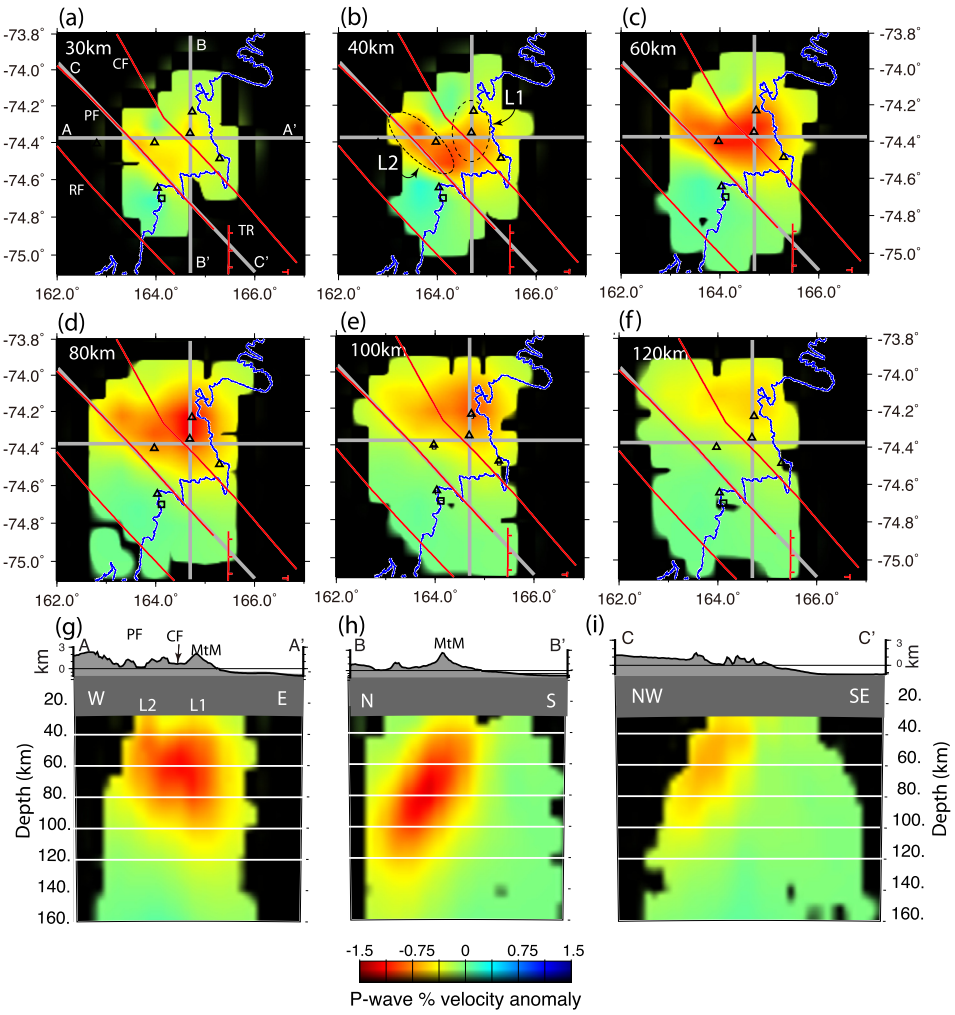

Fig. 4. Recovered model of the inversion with the synthetic travel time residuals computed from the best-input model (Fig. 3): (a)–(f) horizontal cross-sections through the model for depths of 20, 40, 60, 80, 100, and 120 km; (g)–(i) vertical cross-sections for each line in (a).

we found the model that best matched our model inverted from real data (Fig. 3). The best model consisted of two linear low-velocity anomalies that were oriented along the N–S axis beneath Mt. Melbourne (L1) and in the NW direction along the Priestley Fault (L2). The N–S oriented low-velocity anomaly (L1) was generated with 16-km-wide Gaussian spheres starting from a depth of 40–70 km and latitude of −74.4° to −74.2° and with 20-km-wide Gaussian spheres with a −5% slowness anomaly starting from a depth of 70–130 km with 60° dipping to the east and latitude of −74.6° to −74.2° (Fig. 3). The NW-oriented low-velocity anomaly (L2) was produced with 12-km-wide Gaussian spheres centred on the southern tip of the Deep Freeze Range (164.0°E, 74.5°S) and elongated ∼30 km in the NW direction along the Priestley Fault (azimuth ∼320°) with a depth of 20–70 km (Fig. 3).

4. Discussion

The major features of our model were two low-velocity anomalies beneath Mt. Melbourne (L1) and the Deep Freeze Range along the Priestley Fault (L2). As described in Section 3, the low-velocity anomaly beneath Mt. Melbourne was narrow and small at a depth of 30–40 km; it then broadened and extended to the south with dipping to the east up to a depth of 90 km. The N–S trend of the low-velocity anomaly, especially from 60 km to 80 km (Figs. 2(c), (d)), generally correlated well with the topographic height of Mt. Melbourne (Fig. 1) (Wörner and Viereck, 1987, 1989). Regularized tomographic inversion generally reduces the real values of an anomaly with damping and/or smoothing (Lees, 2007). Our resolution test showed that the −5% input anomaly was inverted to a −1.5% anomaly, which suggests that the magnitude of the low-velocity anomaly in our model may have been underestimated by a factor of three (Figs. 3 and 4). Therefore, the observed low-velocity anomaly of about −1.8% beneath Mt. Melbourne (Fig. 2) could be as large as about −5.4%. In mantle tomography, low-velocity anomalies generally indicate the presence of increased temperatures (e.g., Bottinga and Steinmetz, 1979; Jackson et al., 2002; Lees, 2007). Karato (1993) suggested that the seismic wave velocities are dependent on the temperature with corrections for both anharmonicity and anelasticity. Following the method of Karato (1993), we set $Q_P \approx 80$ for the continental rift (Venkataraman et al., 2004) and a −5.4% reduction of the P-wave velocity in our models to calculate a relative temperature increase of 315 K. Armienti and Perinelli (2010) reported the warming of the local lithospheric mantle beneath Mt. Melbourne from 0.5 °C/km for the geothermal gradient to ∼3 °C/km during the development of the Cenozoic magmatism. This indicates a temperature increase of ∼300 °C below a depth of 80 km and the existence of a partial melt at the base of the lithosphere. This high-temperature anomaly is consistent with the increase in the geothermal gradient and suggests the presence of partial melts in the upper mantle (Sato et al., 1988), which could be the heating source for the volcanic activity at Mt. Melbourne.

The other feature of our model was a low-velocity anomaly along the Priestley Fault (L2 in Fig. 2(b)). This anomaly extended to a depth of ~100 km dipping in the NW direction (Fig. 2(i)). The best target resolution test showed that the dipping structure in the NW direction was an artificial structure caused by the smearing-down effect along ray paths by event distributions (Fig. 4(i)). The real structure may be flat up to a depth of ~60 km and parallel to the Priestley Fault (Fig. 3(i)). The Priestley Fault is a major Cenozoic right-lateral fault system that is part of an array of intraplate brittle shear zones extending from the Southern Ocean fracture zones at least in NVL (Salvini et al., 1997). Rocchi et al. (2005) suggested that lithospheric-scale intraplate strike-slip deformation promotes the local decompression melting of the upper mantle source of Cenozoic alkaline magma, which rose and was emplaced along the main NW–SE fault system. The NW–SE low-velocity anomaly in our model did not extend further in the SE direction and could be linked to the low-velocity anomaly beneath Mt. Melbourne at the southern tip of the Deep Freeze Range (Fig. 2(g)).

Mt. Melbourne is located on the eastern flank of the Ross Sea rift, and the location and magmatism of the volcano in NVL are generally accepted to be genetically linked to Ross Sea rifting and the uplift of the Transantarctic Mountains rift shoulder.

As briefly summarized in the introduction, the most recent seismic tomographic study has supported the model of a mantle flow induced by an edge effect in the mantle circulation at the lithospheric step between the thick East Antarctic Craton and thin Ross Sea crust based on structural and morphotectonic analyses (Faccenna et al., 2008), aeromagnetic data (Ferraccioli et al., 2009), and thermobarometry with mantle xenoliths (Armienti and Perinelli, 2010; Perinelli et al., 2011). The edge flow model is also strongly consistent with the E–W fast directions from the seismic anisotropic results (Barklage et al., 2009; Salimbeni et al., 2010). Based on the edge flow model and our tomographic results, we tried to explain the origin of the low-velocity anomalies beneath Mt. Melbourne and the Priestley Fault. In order to infer the shapes of the anomalies from our inversion results, we should consider the spatial distributions of the resolution in addition to the underestimated amplitudes of the anomalies. A resolution test was performed with same input model in Fig. 3 except for L2 coming vertically from a 120 km depth and no dipping to the eastern side of the model; the recovered model was very similar to our best target model, as shown in Fig. 4. The resolution tests revealed limited resolutions for the structure at the eastern edge of the model space and small structures over the entire model space, and we cannot rule out that the anomaly beneath Mt. Melbourne came from deeper depths on the eastern side. Our model showed no low-velocity anomalies below a depth of 120 km, and the low-velocity anomaly beneath the Priestley Fault rose to shallower depths up to ~30 km. One possible mechanism is that the edge-driven convection due to different thicknesses of the lithosphere causes mantle partial melting localized just beneath Mt. Melbourne or the eastern side at a depth of ~110 km. The partially melted material moves up to a depth of 40 km beneath Mt. Melbourne and stretches simultaneously to the southern tip of the Deep Freeze Range at depths of 40–80 km, where the Moho depths are relatively shallow (Di Bona et al., 1997; Yoo et al., 2015). The stretched hot mantle material rises up to a depth of ~30 km and is entrapped at the Priestley Fault. It then flows laterally along the Priestley and Campbell Faults, which are lithospheric right lateral strike-slip faults that were reactivated during the Neogene Period (Fig. 5).

5. Summary

Our P-wave tomographic images revealed two low-velocity anomalies beneath Mt. Melbourne and the Priestley Fault. The low-velocity region under Mt. Melbourne can be attributed to a ~300 °C thermal anomaly at a depth of 80 km. Based on the low-velocity anomalies in our model and the mantle flow model at the lithospheric step between the thick East Antarctic Craton and thin Ross Sea crust, edge-driven convection causes partial melting of the mantle localized beneath Mt. Melbourne or the eastern side at a depth of ~110 km.

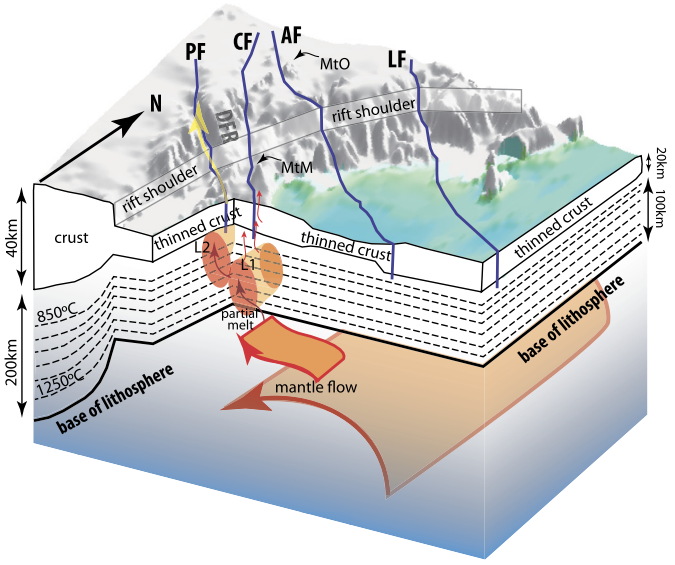

Fig. 5. Block diagram showing our preferred interpretation for the upper mantle thermal anomalies beneath the Mt. Melbourne area. DFR: Deep Freeze Range; PF: Priestley Fault; CF: Campbell Fault; AF: Aviator Fault; LF: Lanteman Fault; MtM: Mt. Melbourne; and MtO: Mt. Overlord. The partially melted mantle (orange areas with red arrows) from the decompressional melt and the edge flow by the lithospheric step between the thick East Antarctic Craton and thin Ross Sea crust moved up and stretched to the southern tip of the DFR. The stretched hot mantle material rose up to a depth of ~30 km and was trapped at PF. It then flowed laterally in the NW direction along the fault line.

Acknowledgement

We thank two anonymous reviewer for constructive comments. This research was supported by a Korea Polar Research Institute Grant (Grant No. PM15020). The TNV seismic data were provided by Programma Nazionale di Ricerche in Antartide (http://panda.bo.ingv.it). Figs. 1, S1, S4, and S5 in this article were generated by the Genetic Mapping Tools 4.5.8.

Appendix A. Supplementary material

Supplementary material related to this article can be found online at http://dx.doi.org/10.1016/j.epsl.2015.10.015.

References

Armienti, P., Perinelli, C., 2010. Cenozoic thermal evolution of lithospheric mantle in northern Victoria Land (Antarctica): evidences from mantle xenoliths. Tectonophysics 486, 28–35.

Bamber, J.L., Gomez-Dans, J.L., Griggs, J.A., 2009. A new 1 km digital elevation model of the Antarctic derived from combined satellite radar and laser data – Part 1: data and methods. Cryosphere 3, 101–111.

Barklage, M., Wiens, D.A., Nyblade, A., Anandakrishnan, S., 2009. Upper mantle seismic anisotropy of South Victoria Land and the Ross Sea coast, Antarctica from SKS and SKKS splitting analysis. Geophys. J. Int. 178, 729–741.

Behrendt, J.C., Blankenship, D.D., Finn, C.A., Bell, R.E., Sweeney, R.E., Hodge, S.M., Brozena, J.M., 1994. CASERTZ aeromagnetic data reveal late Cenozoic flood basalts(?) in the West Antarctic rift system. Geology 22, 527–530.

Behrendt, J.C., LeMasurier, W., Cooper, A., 1992. The West Antarctic rift system—a propagating rift "captured" by a mantle plume. In: Recent Progress in Antarctic Earth Science, pp. 315–322.

Bindschadler, R., Choi, H., Wichlacz, A., Bingham, R., Bohlander, J., Brunt, K., Corr, H., Drews, R., Fricker, H., Hall, M., Hindmarsh, R., Kohler, J., Padman, L., Rack, W., Rotschky, G., Urbini, S., Vornberger, P., Young, N., 2011. Getting around Antarctica: new high-resolution mappings of the grounded and freely-floating boundaries of the Antarctic ice sheet created for the International Polar Year. Cryosphere 5, 569–588.

Bonaccorso, A., Falzone, G., Gambino, S., Privitera, E., 1997. The volcanological observatory of Mount Melbourne, Northern Victoria Land, Antarctica. In: Ricci, C.A. (Ed.), The Antarctic Region: Geological Evolution and Processes. Terra Antarctica Publication, pp. 1083–1086.

Bottinga, Y., Steinmetz, L., 1979. A geophysical, geochemical, petrological model of the sub-marine lithosphere. Tectonophysics 55, 311–347.

Di Bona, M., Amato, A., Azzara, R., Cimini, G.B., Colombo, D., Pondrelli, S., 1997. Constraints on the lithospheric structure beneath the Terra Nova Bay area from teleseismic P to S conversions. In: International Symposium on Antarctic Earth Sciences, vol. 7, pp. 1087–1093.

Faccenna, C., Rossetti, F., Becker, T.W., Danesi, S., Morelli, A., 2008. Recent extension driven by mantle upwelling beneath the Admiralty Mountains (East Antarctica). Tectonics 27, TC4015.

Ferraccioli, F., Armadillo, E., Zunino, A., Bozzo, E., Rocchi, S., Armienti, P., 2009. Magmatic and tectonic patterns over the Northern Victoria Land sector of the Transantarctic Mountains from new aeromagnetic imaging. Tectonophysics 478, 43–61.

Gambino, S., Privitera, E., 1996. Mt. Melbourne volcano, Antarctica: evidence of seismicity related to volcanic activity. Pure Appl. Geophys. 146, 305–318.

Gupta, S., Zhao, D., Rai, S.S., 2009. Seismic imaging of the upper mantle under the Erebus hotspot in Antarctica. Gondwana Res. 16, 109–118.

Hansen, S.E., Graw, J.H., Kenyon, L.M., Nyblade, A.A., Wiens, D.A., Aster, R.C., Huerta, A.D., Anandakrishnan, S., Wilson, T., 2014. Imaging the Antarctic mantle using adaptively parameterized P-wave tomography: evidence for heterogeneous structure beneath West Antarctica. Earth Planet. Sci. Lett. 408, 66–78.

Hole, M., LeMasurier, W., 1994. Tectonic controls on the geochemical composition of Cenozoic, mafic alkaline volcanic rocks from West Antarctica. Contrib. Mineral. Petrol. 117, 187–202.

Jackson, I., Fitz Gerald, J.D., Faul, U.H., Tan, B.H., 2002. Grain-size-sensitive seismic wave attenuation in polycrystalline olivine. J. Geophys. Res., Solid Earth 107.

Karato, S., 1993. Importance of anelasticity in the interpretation of seismic tomography. Geophys. Res. Lett. 20, 1623–1626.

Kennett, B.N.L., Engdahl, E.R., 1991. Travel times for global earthquake location and phase identification. Geophys. J. Int. 105, 429–465.

Keys, J.R., McIntosh, W.C., Kyle, P.R., 1983. Volcanic activity of Mount Melbourne, Northern Victoria Land. Antarctic J. US 18, 10–11.

Kyle, P.R., Moore, J.A., Thirlwall, M.F., 1992. Petrologic evolution of anorthoclase phonolite lavas at Mount Erebus, Ross Island, Antarctica. J. Petrol. 33, 849–875.

Lawrence, J.F., Wiens, D.A., Nyblade, A.A., Anandakrishnan, S., Shore, P.J., Voigt, D., 2006. Rayleigh wave phase velocity analysis of the Ross Sea, Transantarctic Mountains, and East Antarctica from a temporary seismograph array. J. Geophys. Res. 111, B06302.

Lees, J.M., 2007. Seismic tomography of magmatic systems. J. Volcanol. Geotherm. Res. 167, 37–56.

Lyon, G.L., 1986. Stable isotope stratigraphy of ice cores and the age of the last eruption at Mount Melbourne, Antarctica. N.Z. J. Geol. Geophys. 29, 135–138.

Morelli, A., Danesi, S., 2004. Seismological imaging of the Antarctic continental lithosphere: a review. Glob. Planet. Change 42, 155–165.

Nathan, S., Schulte, F.J., 1967. Recent thermal and volcanic activity on Mount Melbourne, Northern Victoria Land, Antarctica. N.Z. J. Geol. Geophys. 10, 422–430.

Park, Y., Yoo, H.J., Lee, W.S., Lee, J., Kim, Y., Lee, S.H., Shin, D., Park, H., 2014. Deployment and performance of a broadband seismic network near the New Korean Jang Bogo research station, Terra Nova Bay, East Antarctica. Seismol. Res. Lett. 85, 1341–1347.

Perinelli, C., Armienti, P., Dallai, L., 2011. Thermal evolution of the lithosphere in a rift environment as inferred from the geochemistry of mantle cumulates, Northern Victoria Land, Antarctica. J. Petrol. 52, 665–690.

Rocchi, S., Armienti, P., D'Orazio, M., Tonarini, S., Wijbrans, J.R., Di Vincenzo, G., 2002. Cenozoic magmatism in the western Ross Embayment: role of mantle plume versus plate dynamics in the development of the West Antarctic Rift System. J. Geophys. Res., Solid Earth 107, 2195.

Rocchi, S., Armienti, P., Di Vincenzo, G., 2005. No plume, no rift magmatism in the West Antarctic Rift. Spec. Pap., Geol. Soc. Am. 388, 435–447.

Rocchi, S., Storti, F., Di Vincenzo, G., Rossetti, F., 2003. Intraplate strike-slip tectonics as an alternative to mantle plume activity for the Cenozoic rift magmatism in the Ross Sea region, Antarctica. Geol. Soc. (Lond.) Spec. Publ. 210, 145–158.

Rossetti, F., Storti, F., Salvini, F., 2000. Cenozoic noncoaxial transtension along the western shoulder of the Ross Sea, Antarctica, and the emplacement of McMurdo dyke arrays. Terra Nova 12, 60–66.

Salimbeni, S., Pondrelli, S., Danesi, S., Morelli, A., 2010. Seismic anisotropy of the Victoria Land region, Antarctica. Geophys. J. Int. 182, 421–432.

Salvini, F., Brancolini, G., Busetti, M., Storti, F., Mazzarini, F., Coren, F., 1997. Cenozoic geodynamics of the Ross Sea region, Antarctica: crustal extension, intraplate strike-slip faulting, and tectonic inheritance. J. Geophys. Res., Solid Earth 102, 24669–24696.

Sato, H., Sacks, I.S., Murase, T., Scarfe, C.M., 1988. Thermal structure of the low velocity zone derived from laboratory and seismic investigations. Geophys. Res. Lett. 15, 1227–1230.

Sieminski, A., Debayle, E., Lévêque, J.-J., 2003. Seismic evidence for deep low-velocity anomalies in the transition zone beneath West Antarctica. Earth Planet. Sci. Lett. 216, 645–661.

Storey, B.C., Leat, P.T., Weaver, S.D., Pankhurst, R.J., Bradshaw, J.D., Kelley, S., 1999. Mantle plumes and Antarctica–New Zealand rifting: evidence from mid-Cretaceous mafic dykes. J. Geol. Soc. 156, 659–671.

Storti, F., Rossetti, F., Salvini, F., 2001. Structural architecture and displacement accommodation mechanisms at the termination of the Priestley Fault, Northern Victoria Land, Antarctica. Tectonophysics 341, 141–161.

VanDecar, J.C., 1991. Upper mantle structure of the Cascadia subduction zone from non-linear teleseismic travel time inversion. Univ. of Washington, Seattle, WA.

VanDecar, J.C., Crosson, R.S., 1990. Determination of teleseismic relative phase arrival times using multi-channel cross-correlation and least-squares. Bull. Seismol. Soc. Am. 80, 150–169.

Venkataraman, A., Nyblade, A.A., Ritsema, J., 2004. Upper mantle Q and thermal structure beneath Tanzania, East Africa from teleseismic P wave spectra. Geophys. Res. Lett. 31.

Watson, T., Nyblade, A., Wiens, D.A., Anandakrishnan, S., Benoit, M., Shore, P.J., Voigt, D., VanDecar, J., 2006. P and S velocity structure of the upper mantle beneath the Transantarctic Mountains, East Antarctic craton, and Ross Sea from travel time tomography. Geochem. Geophys. Geosyst. 7.

Wörner, G., Viereck, L., 1987. Subglacial to emergent volcanism at Shield Nunatak, Mt. Melbourne volcanic field, Antarctica. Polarforschung, Bremerhaven, Alfred Wegener Institute for Polar and Marine Research & German Society of Polar Research 57, 27–47.

Wörner, G., Viereck, L., 1989. Mount Melbourne. In: E., L.W., W., T.J. (Eds.), Volcanoes of the Antarctic Plate and Southern Oceans. AGU Antarctic Research Series, pp. 72–78.

Yoo, H.J., Park, Y., Lee, S.-H., Lee, W.S., Yun, S., Lee, C.-k., Kim, Y., Park, H., 2015. Crustal and upper mantle structure beneath Mt. Melbourne, Antarctica: implications for partial melting. Unpublished manuscript.